# OmniResMonitor: omnimonitoring of human respiration using acoustic multipath reflection

Tianben Wang, Zhishen Wang, Xiantao Liu, Wenbo Liu, Leye Wang, Yuanqing Zheng, Jin Hu, Tao Gu, Daqing Zhang

# OmniResMonitor: Omnimonitoring of Human Respiration using Acoustic Multipath Reflection

Tianben Wang, Zhishen Wang, Xiantao Liu, Wenbo Liu, Leye Wang, Yuanqing Zheng, Jin Hu, Tao Gu, *Member, IEEE*, Daqing Zhang, Fellow, IEEE.

**Abstract**—Contactless respiration monitoring using wireless signals has drawn much attention in recent years. Many approaches have been proposed, however, they may not work when there is a lack of signals directly reflected from target's chest, e.g., a target faces away from the transceiver or a target is blocked by furniture. In this paper, we design and implement a novel omnimonitoring system for human respiration, *OmniRespMonitor*, using a pair of speaker and microphone. Different from Radio Frequency (RF) signal, acoustic signals cannot penetrate through walls and furniture. The multipath reflection in an indoor environment will result in highly abundant acoustic signals. In this case, even though there are lack of acoustic signals directly reflected by a target's chest, indirectly-reflected acoustic signals can still be received by the microphone. We can therefore monitor the target's respiration by extracting this subtle variation of indirectly reflected signals. To achieve this, we model chest movement using truncated System Frequency Response (SFR). We then develop a global search method based on the autocorrelation function to extract minute chest movement from SFR sequences. Finally, we dynamically synthesize the chest movement information to recover the breathing wave in real time. We conduct extensive experiments with both humans and animals (goat), the results show that *OmniResMonitor* is able to monitor single target's respiration within 5 meters in indoor environments in various challenging scenarios there are lack of directly-reflected acoustic signals.

**Index Terms**—Acoustic Sensing, Contactless Respiration Monitoring, System Frequency Response

## 1 Introduction

RISPIRATION is one of the basic vital signs of human being. Chronic respiratory diseases (CRDs) such as Apnea and chronic obstructive pulmonary disease (COPD) are quite common among the elders [6]. COPD is the fourth leading cause of death worldwide, which affects about 300 million people worldwide and more than 3 million people die from COPD every year [6,7]. Continuous respiration monitoring in home settings is crucial to trigger early warnings and prevent death.

The respiration monitoring devices in clinic settings such as thoracic impedance pneumography [8], capnography [9] or pulse oximeter [10] can accurately monitor human respiration. However, these devices are usually intrusive and inconvenient to use in a home setting. In addition, they require well-trained professionals to set up and assist users to wear and operate properly. Commercial wearable devices have been largely deployed to monitor human respiration [11, 12]. However, wearable devices are generally intrusive and they may have a low level of user acceptance and poor usability.

Researchers has recently turned their attention to contactless sensing, i.e., non-intrusive respiration monitoring, including laser [13, 14], microwave [18], RFID [4, 19-21], Doppler radar [24, 25], FMCW radar [1, 55], UWB radar [26, 27, 54], customized RF devices [28, 29], commodity camera [15-17], Zigbee [22, 23], WiFi [2, 5, 30, 31, 33-41] and audio devices [3,43-47]. Although these research studies show great promise in monitoring human respiration using a variety of wireless signals, they usually require that a receiver is able to receive the signals directly reflected from a target's chest. This is often not the case in real-world scenarios, e.g., a target is located outside the transmission area of a transceiver, a target faces away from transceiver, or is blocked by the furniture. A recent study done by Liu et al [42] attempts to tackle this problem using smartphone and a WiFi router. Their system is able to work in non-line-of-Sight (NLoS) scenarios, however it requires that the smartphone is close to the subject, i.e., tens of centimeters. In addition, the system only works offline, not in real time. Liu et al [32] also propose to monitor respiration at different sleeping postures leveraging WiFi's Channel Frequency Response (CFR), however their system requires three pairs of transceivers around the subject to cover different postures.

In this paper, we design and implement an acoustic-based omnimonitoring system, *OmniResMonitor*, using a


- *T. Wang, X. Liu, W. Liu and J. Hu are with the College of Mechanical and Electronic Engineering, Northwest A&F University, Yangling 712100, China and Key Laboratory of Agricultural Internet of Things, Ministry of Agriculture and Rural Affairs, Yangling, 712100, China; E-mail: wangtb@nwafu.edu.cn; liuxt@nwafu.edu.cn; 15039854668@163.com; hujin007@nwsuaf.edu.cn.*
- *Z. Wang is with Center of Ultra-Precision Optoelectronic Instrument, Harbin Institute of Technology, Harbin 150080, China. E-mail: 21B901035@stu.hit.edu.cn.*
- *L. Wang is with School of EECS, Peking University, China. E-mail: leyewang@pku.edu.cn.*
- *Y. Zheng is with the Department of Computing, the Hong Kong Polytechnic University, Hung Hom, Kowloon, Hong Kong. E-mail: csyqzheng@comp.polyu.edu.hk.*
- *T. Gu is with Department of Computing at Macquarie University, Australia. E-mail: tao.gu@mq.edu.au.*
- *D. Zhang and L. Wang are with Département Réseaux et Services Multimédia Mobiles, Telecom SudParis, France. Email: daqing.zhang@telecom-sudparis.eu.*

pair of speaker and microphone. The system is able to accurately monitor target's respiration even when there is a lack of directly-reflected signals from target's chest. Different from RF signals, acoustic signals cannot penetrate through walls and furniture. The transmitted signal is mainly reflected by the ambient environment. Due to abundant multipath reflection, regardless of the transceiver's location and orientation, the microphone can always receive the signal indirectly reflected by human chest. Our intuition is to exploit acoustic multipath reflection, especially the signal indirectly reflected from target's chest to address location and orientation sensitive issue. To achieve this, we first capture the minute-level variation of multipath reflection signals caused by chest movement. We then recover the breath wave by dynamically synthesizing the variation. However, this is not a trivial task due to several challenges.

(1) In the case that a target faces away from the transceiver or is blocked by furniture, since there is no signal directly reflected from the targets' chest. We can use indirectly reflected signals (via walls, ceilings and furniture). However, due to multipath reflections and a longer propagation distance, the power of indirectly reflected signal can be very weak. What's worse, the inherent variation of transmitted signal caused by the nonlinearity of electronic components and inevitable ambient noise will also result in variation of indirectly reflected signal. Hence, it is challenging to extract chest movement from weak and interfered indirectly reflected signals.

(2) Due to different reflection paths and different reflection points on the chest, each indirectly reflected multipath signal varies with different amplitudes and phases. How we synthesize the variation of these indirectly reflected multipath signals to recover breath wave is challenging.

To address the aforementioned challenges, we firstly model chest movement using truncated system frequency response (SFR), which is defined as the ratio of transmitting signal and receiving signal at different frequencies. It is able to not only accurately quantify the amplitude of all multipath signals (including direct and indirect signals reflected by the chest) with different frequencies but also shield the interference caused by noise and the inherent variation of transmitted signals. We then propose a global searching method based on autocorrelation to extract minute-level chest movement information from the variation over time of the points in SFR. Finally, we design a novel algorithm to recover breath wave by synthesizing chest movement in real time. The main contributions of this paper can be summarized as follows.

(1) We design and implement an omnimonitoring system for human respiration, *OmniResMonitor*, using only a pair of speaker and microphone. We propose truncated SFR to model minute-level chest movement and globally search all the multipath signals indirectly reflected from target's chest from the truncated SFR sequence leveraging autocorrelation. In this way, *OmniResMonitor* can accurately monitor human respiration in indoor environments when there are no signals directly reflected from the target's chest.

(2) We conduct extensive experiments to evaluate *OmniResMonitor* in various indoor scenarios including three challenge scenarios: 1) the transceiver faces the target's back, 2) the target and the transceiver face away from each other, 3) the target is blocked by obstacles. We also evaluate *OmniResMonitor* with animal, i.e., 4 goats of different ages and sizes. Experimental results show that *OmniResMonitor* accurately monitors subject's respiration 5 meters away from the transceiver in the scenarios that there are no signals directly reflected from the target's chest.

## 2 Related Work

In this section, we discuss the work related to contactless respiration monitoring. According to type of signals used, existing work can be grouped into three categories: RF device-based, commercial WiFi-based, and acoustic device-based.

### 2.1. RF Device-based

RF device-based technologies ranging from microwave [18], RFID [4,19-21], Zigbee [22,23], Doppler radar [24,25], FMCW radar [1], UWB radar [26,27,54], customized RF devices [28,29] have been proposed to detect human respiration. The work [55] can even eliminate the impact of body movement. The basic idea is to directly measure chest movement displacement during respiration with RF signals. Although these methods achieve accurate respiration detection in some specific scenarios, they typically rely on signals directly reflected from target's chest. They generally do not work well in the scenarios where there is no signal directly reflected from target's chest.

### 2.2. Commercial WiFi-based

In WiFi sensing, received signal strength (RSS) has been exploited for monitoring respiration. Abdelnasser et al. [30] first attempt to monitor human respiration leveraging the amplitude change of RSS. Similar work includes WiBreathe [31] and Breathfinding [48]. However, due to low distance resolution, RSS-based approaches cannot effectively detect minute-level chest movement and they are vulnerable to ambient noise. Compared with RSS, CSI has a higher distance resolution and it is more sensitive to chest displacement. PhaseBeat [50], TensorBeat [51] and studies in [33-35] successfully track respiration using CSI. These approaches are able to detect respiration in specific settings, but their studies are mostly based on experiments, and they do not quantify the relationship between CSI variation and chest movement displacement. Zhang, et al. [36,49] first introduce the Fresnel Zone model to monitor respiration. They demonstrate the quantitative relationship between CSI variation and chest movement displacement. The same model has been applied in [2,5,37-40] to further improve the performance of respiration monitoring from a range of aspects. To monitor respiration for multiple subjects simultaneously, Zeng, et al. [41] use independent component analysis (ICA) to separate the reparation information for each subject. However, these works rely on signals directly reflected from subject's chest. This may not be the case in reality, e.g., a subject faces away

from the transceiver, an obstacle blocks reflected signals. WiPhone [42] is a smartphone based respiration monitoring system that works in a non-line-of-Sight (NLoS) scenario leveraging WiFi multipath reflection. However, the smartphone need to be placed close to the subject (i.e., less than a meter) to ensure strong reflected signals. In addition, the system works offline, not sure if it works in real time. WiSleep [32] is the first system that tracks respiration while a subject is sleeping with different postures using multipath reflected WiFi signals. The system has demonstrated that the effectiveness of frequency response in extracting multipath reflection signals in indoor environments to reduce blind spots. However, the system requires three pairs of Tx and Rx around the target to cover different postures.

### 2.3. Acoustic Device-based

Acoustic-based approaches have recently attracted research attention. Acoustic signal can be easily found in daily life. Arlotto et al., [46] monitor respiration by sensing exhaled airflow during respiration. Wang et al., [3] implement a similar idea using a commodity audio device and improve the performance by modeling the angle variation between the direction of exhaled airflow and the direction of acoustic beam. These two approaches require that the acoustic beam directly covers the area around a subject's mouth and nose. Except for sensing exhaled airflow, Nandakumar et al., [43] transform a smartphone into an FMCW sonar to measure chest movement displacement during respiration. However, its ranging accuracy is limited by the narrow frequency band of smartphones. To improve accuracy, Min et al., [44] use 240 kHz ultrasonic pulse to measure chest movement. Even though it achieves a high ranging accuracy, the approach requires expensive ultrasonic transceivers. To obtain high ranging accuracy using commodity audio devices, Wang et al., [45] propose C-FMCW, which accurately estimates chest movement during respiration using commodity speaker and microphone. To expand the measurable angle, Wang et al., [47] exploit beamforming based on a microphone array to capture the respiration of infant. The system can capture an infant's respiration within 90°. Xu et al., [52] propose a fine-grained breathing monitoring system BreathListener, which is able to recover the breath wave and shield the influence of body sway in driving environments. Wan RespTracker [53] is the first multi-target acoustic respiration monitoring system. It can simultaneously monitor multiple targets' respiration. **However, all the above acoustic respiration monitoring systems rely on the signals directly reflected from target's chest. They fail when a target faces away from the transceiver or is blocked by an obstacle between device and subject.**

*OmniResMonitor* fully leverages abundant acoustic multipath reflection to monitor a single target's respiration focusing on the challenge scenarios where there are no signals directly reflected from target's chest.

## 3 System Design

### 3.1 Design Motivation and System Framework

We consider a scenario where there are two people in a room and they face away from each other or both are blocked by indoor furniture. In these scenarios, one can still hear what the other says since the voice signals may be reflected from the static environment and propagate through multipath. We may extract usefully information from indirectly-reflected acoustic signals. A target's chest movement during respiration will periodically change the amplitude and propagation path of multipath signals which can be viewed as system parameters. Thus, if we can estimate the system parameters to quantify variation of multipath signal in real time, we can then extract target's respiration.

Based on the above basic idea, we deign our system as shown in Fig. 1. Firstly, we use speaker to transmit a sinusoidal frequency modulated signal. The reflected acoustic signal from the environment and the target's chest are received by the microphone. Based on the transmitted and echo frame, we estimate system parameters–truncated SFR, which describes the amplitude of all multipath signals including direct and indirect reflected signals with different frequencies. Thus, the SFRs over time is able to depict the variation of all multipath signals. The chest movement during breathing is usually periodical, hence the reflection paths directly and indirectly affected by the subject' chest movement vary periodically over time, but the paths reflected from the ambient environment show no periodicity. Based on the above idea, we separate the multipath signals corresponding to the subject' chest movement by selecting all the periodical SFR sequences (defined in Sec. 3.2.2). Finally, we normalize and synchronize these periodical SRF sequences to recover the breath wave in real time.

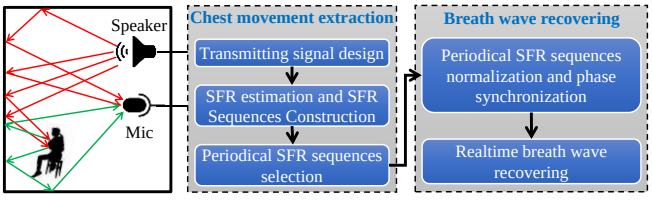


Fig. 1. Framework of *OmniResMonitor*

### 3.2 Chest Movement Extraction

#### 3.2.1 Transmitted Signal Design

To estimate SFR, the transmitted signal should be designed with a wide frequency band. Though FMCW signals show an advantage in distance resolution due to linear relationship between frequency difference and distance, it may still introduce audible noise due to its discontinuous phase variation over time. To avoid the noise embedded in transmitting signals, we design the transmitting signal as a sinusoidal frequency modulated signal whose phase variation over time is smooth and continuous. The frequency of the transmitted signal at time $t$ is given by:

$$f(t) = f_c + \frac{B}{2}\left(1 + sin(2\pi t/T)\right), 0 \le t \le T \qquad (1)$$

where $f_c$, $B$ and $T$ denote carrier frequency, modulation bandwidth, and modulation period, respectively. In order to avoid audible noise, $f_c$ should be higher than 18KHz. The phase is the integral of $f(t)$ over time.

$$u(t) = 2\pi \int_0^t f(t')dt' = 2\pi \left( f_c t + \frac{Bt}{2} - \frac{BT}{4\pi} cos(2\pi t/T) \right) \quad (2)$$

Then, the transmitted signal can be presented as $x_t(t) = cos\big(u(t)\big)$.

In order to estimate $H(k)$, we have to obtain one full echo of a transmitted signal. However, during respiration monitoring, we have to transmit $x_t(t)$ continuously. The problem of multipath delay may rise, and one echo will be overlapped by neighboring echoes. In other words, the echo we received is an overlapped version of several neighboring echoes. It will lead to wrong SFR estimation. To tackle this problem, the transmitted signal is modified as a pulse with a duty cycle.

$$x_t(t) = \begin{cases} \cos\big(u(t)\big)h(t), & 0 \le t \le T \\ 0, & T < t \le T' \end{cases} \quad (3)$$

where $h(t)$ is a Hanning window, which is applied to mitigate spectrum leakage caused by sudden amplitude changes. $T'$ is the period of the modified transmitted signal, $T' > T$. To avoid echo overlap, $T' - T$ should be larger than multipath delay. Generally, a larger room has a larger multipath delay and requires a larger $T' - T$. The discrete transmitted signal is finally represented as follows.

$$x_t(n) = \begin{cases} \cos\big(u(nT_s)\big)h(t), & 0 \le nT_s \le T \\ 0, & T < nT_s \le T' \end{cases} \quad (4)$$

where $T_s = 1/f_s$ is the sampling interval.

The iteration frequency of *OmniResMonitor* is $f_s' = 1/T'$. Generally, $f_s^{'} = 10$ Hz is adequate for monitoring respiration signals that have a typical frequency of 0.17 ~ 0.42 Hz, i.e., 10 ~ 25 bpm. Thus, $T'$ is recommended as 0.1 second. According to our preliminary test, multipath delay, i.e., $T^{'} - T$ is within 0.03 ~ 0.06 second in the room with a size of 20 ~ 60 m². A larger room generally has a larger multipath delay thus requiring smaller $T$. Larger modulation bandwidth, i.e., $B$ means more elaborate multipath signal quantification, while introduce larger computation burden of effective multipath signal separation (refer to Eq. 6). In order to run *OmniResMonitor* on laptop in real time, $B$ is recommended as 2K ~3KHz. Fig. 2 shows an example of the transmitting signal ($f_s = 96KHz$, $f_c = 26KHz$, $B = 2KHz$, $T = 0.05s$, $T' = 0.1s$).

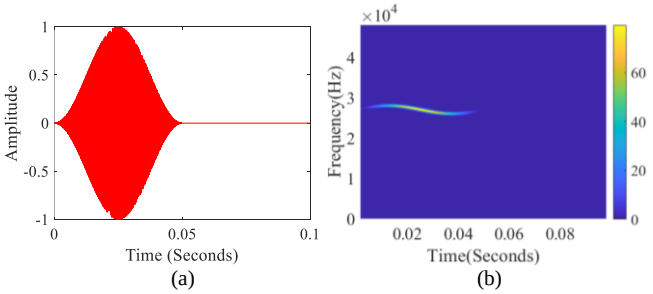


(a) (b)

Fig. 2. An example of the transmitted signal. (a) time-domain signal. (b) Short-time Fourier transform of (a)

*OmniResMonitor* controls the transceiver to continuously transmit the designed signal and receive the echo frame. Specifically, the designed signal is continuously transmitted by the speaker in a non-blocking manner, and meanwhile, the microphone receives the echo frame synchronously. The length of the echo frame has to be the same as that of the transmitting signal.

### 3.2.2 SFR Estimation and SFR Sequence Construction

With the transmitted signal $x_t(n)$ (refer to Eq. 4) and the echo frame $x_r(n)$, SFR is estimated as:

$$H(k) = \frac{X_r(k)}{X_t(k)} = \frac{DFT\big(x_r(n)\big)}{DFT\big(x_t(n)\big)} \quad (5)$$

where $H(k)$ is the SFR at frequency $f = k\Delta f = k\frac{f_s}{N}, k = 1,2,\dots,N/2$, $N$ is the length of $x_r(n)$. $DFT()$ denotes discrete Fourier transform.

To eliminate noise interference beyond the frequency band of the transmitted signal, we only retain SFR within frequency band $[f_c, f_c + B]$, i.e., $f_c \le f \le f_c + B$. Plugging in $f = k\frac{f_s}{N}$, we obtain the range of $k$ as $\frac{Nf_c}{f_s} \le k \le \frac{N(f_c+B)}{f_s}$. Thus, the SFR at time $t$ is truncated as:

$$\boldsymbol{H_t} = \left[ H\left(\left\lceil \frac{Nf_c}{f_s} \right\rceil\right), H\left(\left\lceil \frac{Nf_c}{f_s} \right\rceil + 1\right), \dots, H\left(\left\lfloor \frac{N(f_c+B)}{f_s} \right\rfloor\right) \right]^T \quad (6)$$

The SFRs over time form a matrix called as SFR matrix, which can be represented as:

$$\boldsymbol{S} = [H_{t_1}, H_{t_2}, \dots, H_{t_m}] \quad (7)$$

where $t_1, t_2, \dots, t_m$ are the time stamp that *OmniResMonitor* computes SFR in each iteration cycle (*OmniResMonitor* runs for one time). Generally, the duration of each iteration cycle is about $T'$ (the period of the modified transmitted signal. Refer to Eq. 3). Let $\boldsymbol{S_i}$ $(i = 1, 2, \dots, \left\lfloor \frac{N(f_c+B)}{f_s} \right\rfloor - \left\lceil \frac{Nf_c}{f_s} \right\rceil + 1)$ denote the i-th row of $\boldsymbol{S}$. From Eq. 7, we know that $\boldsymbol{S_i}$ denotes the amplitude variation over time of multipath signal with frequency $f = \frac{f_s}{N}\left(i + \left\lceil \frac{Nf_c}{f_s} \right\rceil - 1\right)$. Here, we call $\boldsymbol{S}_i$ one SFR sequence. Fig. 3 shows the SFR sequences (i.e., rows of matrix $\boldsymbol{S}$) when a subject is breathing naturally in the room (the parameters of the transmitted signal are the same as that in Fig. 2).

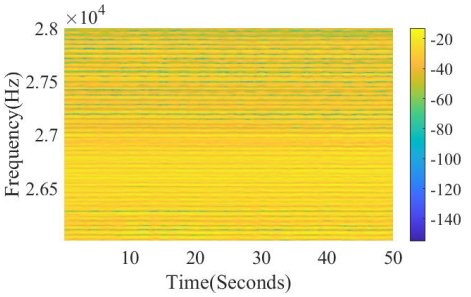


Fig. 3. An example of SFR sequences

In each iteration cycle of *OmniResMonitor*, matrix $\boldsymbol{S}$ is updated. The SFR estimated in current iteration cycle is added as a new column to the end of $\boldsymbol{S}$, and the first column of $\boldsymbol{S}$ is eliminated.

### 3.2.3 Effective Multipath Signal Separation based on Periodical SFR Sequences Selection

Human respiration is periodical in nature. It means that the SFR sequences corresponding to chest movement during respiration vary periodically. We select all the SFR sequences that vary periodically by measuring their periodicity. Specifically, we first detrend the nonlinear trend of all SFR sequences. Then, we calculate the autocorrelation of all SFR sequences. Finally, based on the autocorrelation results, the SFR sequences that have strong periodicity are selected.

### 1) SFR Sequences Detrending

Due to the fact that audio device is not a strictly linear system, the SFR sequence is embedded with a nonlinear trend, which will not only decrease the periodicity of the SFR sequences, resulting in loss of chest movement information, but also affect breath wave recovering.

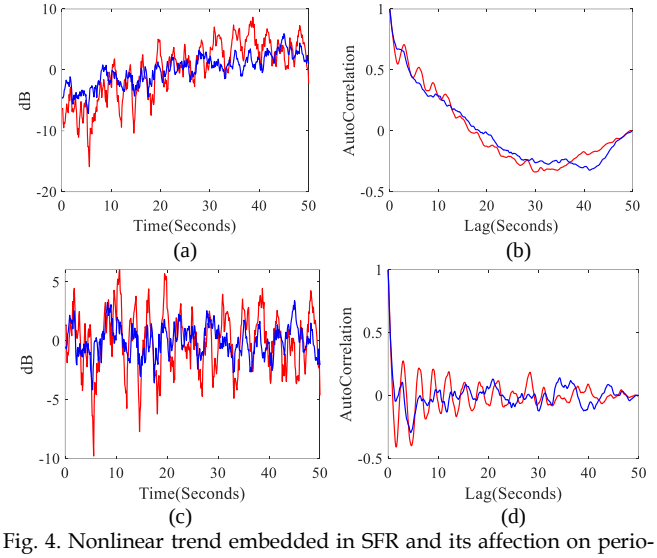


Fig. 4. Nonlinear trend embedded in SFR and its affection on periodicity. (a) two SFR sequences embedded with the nonlinear trend. (b) autocorrelation of the two SFR sequences shown in (a). (c) two SFR sequences after detrending. (d) autocorrelation of the two SFR sequences after detrending.

Fig. 4(a) shows two SFR sequences. The red line has obvious periodicity, while the blue line is aperiodic. However, due to the impact of the nonlinear trend, their autocorrelation results shown in Fig. 4(b) are very similar. It is difficult to select effective SFR sequences using autocorrelation.

To tackle this problem, we have to remove the trend of the SFR sequence. Firstly, we extract the polynomial trend of each SFR sequence using the Least Square method. Then, the polynomial trend is subtracted from each SFR sequence. Extensive preliminary experiments indicate that quartic polynomial is enough to eliminate all the nonlinear trends. Fig. 4(c) shows the detrending result of two SFR sequences in Fig. 4(a). The autocorrelations of two detrended SFR sequences are shown in Fig. 4(d). Obviously, the autocorrelations of two detrended sequences are significantly different. It is easy to select the strong periodical sequence using the simple rule that a higher peak of the autocorrelation function means stronger periodicity.

### 2) Autocorrelation of SFR Sequence

After detrending, we measure the periodicity of all SFR sequences using autocorrelation. The autocorrelation of $\boldsymbol{S_i}$ is defined as:

$$R_x(k) = \frac{c_k}{c_0} \tag{8}$$

where $c_k$ is the auto-covariance of $\boldsymbol{S_i}$,

$$c_k = \frac{1}{N}\sum_{n=1}^{N-k}(\boldsymbol{S_i}(n) - \bar{\boldsymbol{S_i}})(\boldsymbol{S_i}(n+k) - \bar{\boldsymbol{S_i}}) \tag{9}$$

where $k = 0,1,\dots,N-1$. As shown in Fig. 4(d), the autocorrelation of the periodical sequence looks like a sinusoid but amplitude decreases gradually, while the autocorrelation of the aperiodic sequence varies irregularly.

### 3) Periodical SFR Sequences Selection

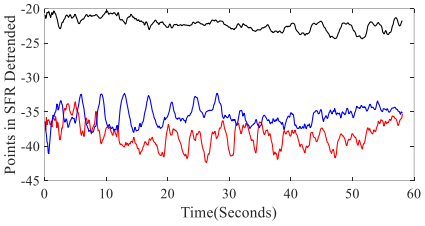


Fig. 5. Dynamic change of the periodicity of SFR sequences.

Fig. 5 shows three SFR sequences of one minute. We observe that their periodicity changes over time. The SFR sequence colored blue shows relatively strong periodicity in the beginning, while the SFR sequences colored red and black show relatively strong periodicity in the middle and end, respectively. In other word, none of SFR sequences can always correspond to chest movement. To address this problem, we introduce a 20 second sliding window. Specifically, in each iteration cycle (*OmniResMonitor* runs for one time), we only calculate the autocorrelation of latest 20 seconds (human respiration rate is 12~25 bmp. 20 seconds contains at least 4 breaths) SFR sequences. Based on the autocorrelation, the SFR sequences that have relatively strong periodicity are selected with the following rules. According to the definition of autocorrelation and the example shown in Fig. 4(d), comparing with the sequence with weak or without periodicity, the autocorrelation function of sequence with relatively strong periodicity shows two notable characteristics:

1) The peaks of the autocorrelation function are relatively high. Higher peaks mean higher similarity of chest movement displacement variation during each respiration cycle (containing a full inhale and a full exhale).

2) The intervals of peak lags are almost the same. Closer interval values mean higher similarity of the length of all respiration cycles.

Based on the above characteristics, we define the rules to select the effective SFR sequence. Suppose the first four peaks of the autocorrelation of one SFR sequence are $[(p_1, l_1), (p_2, l_2), (p_3, l_3), (p_4, l_4)]$, then the peak intervals are $[l_1, l_2 - l_1, l_3 - l_2, l_4 - l_3]$. The rules are built as follows to judge whether it's periodical:

$$\begin{cases} p_1 > PkThrd, & and \\ max(intervals) - min(intervals) < \dfrac{ItvlThrd \cdot MidD}{T'} \end{cases}$$

where $T'$ is the duration of a single transmitting time slot (refer to Eq. 5). $MidD = 3.7$ seconds is the mid-value of one breath duration (human respiration rate is 12~25 bmp). According to extensive experimental analysis, both $PkThrd$ and $IntervalThrd$ are set to 0.2~0.25. Specifically, the experimental result shows that $0.2 \le PkThrd \le 0.25$ is a good promise to select the effective SFR sequence. This implies that the relative difference of the length of four consecutive respiration cycles should not be larger than $1/4$. Note that even one's respiration rate is changing rapidly, the relative difference of the length of four consecutive respiration cycles will not be larger than $1/4$. In other words, $0.2 \le ItvlThrd \le 0.25$ can adapt to the normal respiration rate change, and shield the SFR sequence with poor periodicity.

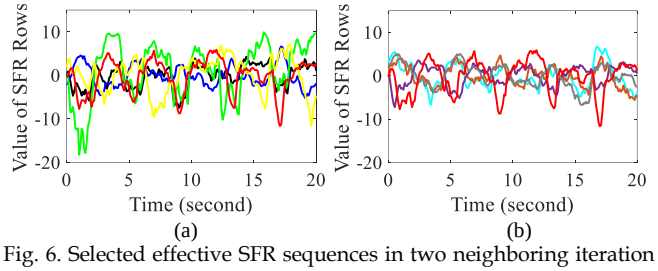


Fig. 6. Selected effective SFR sequences in two neighboring iteration cycles. (a) Selected effective SFR sequences in the last iteration cycle. (b) Selected effective SFR sequences in the current iteration cycle.

In order to reduce the information redundancy and computational burden of subsequent procedures, we only retain the effective SFR sequences whose $p_1$ is ranked in the top 5. If the number of periodical SFR sequences is less than 5, all the periodical SFR sequences are retained. Fig. 6 shows an example of the selected effective SFR sequences in two neighboring iteration cycles (iteration cycle duration of this example is about 0.1 s). We can observe that:

- *OmniResMonitor* selects effective SFR sequences dynamically. Except for the SFR sequence highlighted with a red line in Fig. 6(a) and Fig. 6(b), the effective SFR sequences selected in two neighboring iteration cycles are different.
- None of the single SFR sequences has enough periodicity to describe the subject's respiration. It means that we have to fuse the effective SFR sequences to recover breath waves.

The advantages of the above method are summaries as follows:

(1) It simultaneously extracts the signal directly and indirectly reflected from the subject's chest.
(2) It is able to catch very weak indirectly reflected signals because the selecting process based on periodicity measuring is independent from the signal amplitude.
(3) Measuring the periodicity of SFR sequence rather than the spectral purity of SFR sequence allows this method to catch the multipath signal with complex periodical variation, e.g., periodic square wave, periodic pulse or even arbitrary periodic curve.

These advantages ensure the extraction of indirectly reflected signals in challenging scenarios, e.g., the subject faces away from the transceiver, or is blocked by an obstacle.

### 3.3 Breath Wave Recovering

We recover breath wave by dynamically synthesizing the selected effective SFR sequences. We observe from Fig. 6 that the selected SFR sequences have different amplitudes. Directly adding these SFR sequences will weaken the contribution of the SFR sequences with relatively high periodicity but small amplitude. In addition, some of the SFR sequences have opposite phases, i.e., their phase difference is π. In Fig. 6 (a), according to the variation direction over time, the SFR sequences can be divided into two categories. The first category includes the SFR sequences highlighted with green, red, and black, and the second category includes the other SFR sequences. We can see that the SFR sequences that belong to the same category have the almost same phase, and the phase difference between the two categories is about π. The same phenomenon can be observed in Fig. 6 (b). Directly adding these SFR sequences to recover breath wave will result in that the SFR sequences have opposite phases cancel each other out, and finally lead to poorly recovered breath wave.

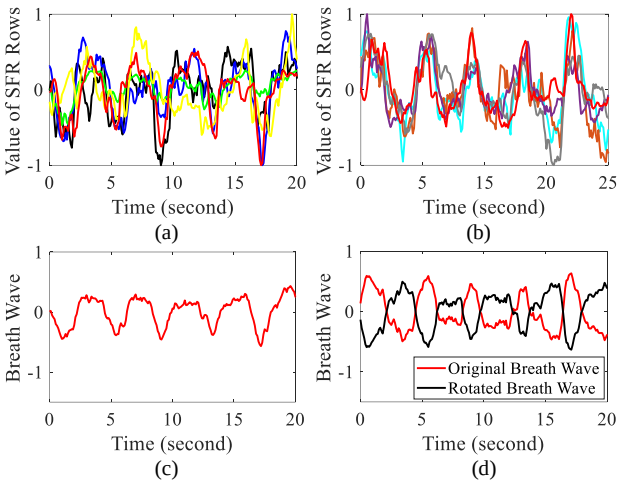


Fig. 7. Breath wave recovering. (a) Effective SFR sequences after normalization and phase synchronization in the last iteration cycle. (b) Effective SFR sequences after normalization and phase synchronization in current iteration cycle. (c) Breath wave recovered in last iteration cycle. (d) Breath wave recovered in current iteration cycle.

To tackle the above problems, we firstly normalize all SFR sequences. Then, we synchronize the phase of the SFR sequences by rotating part of them along the time axis (refer to Algorithm 1). Finally, the SFR sequences are added together to build breath wave. Fig. 7 (a) and Fig. 7 (b) show effective SFR sequences selected in Fig. 6 (a) and Fig. 6 (b) after normalization and phase synchronization, respectively. The red lines in Fig. 7 (c) and Fig. 7 (d) show the recovered breath wave recovered from Fig. 7 (a) and Fig. 7 (b), respectively. Now, we can clearly distinguish each breath.

The recovered breath wave highlighted with red lines in Fig. 7 (c) and Fig. 7 (d) are neighboring in time. They are generated in two adjacent iteration cycles of *OmniResMonitor*. But we observe that their phases are composite. In order to ensure that the recovered real time breathing wave is continuous over time, we should ensure the phases of the breath wave recovered in two adjacent iteration cycles

are close. Specifically, if the phase difference between the recovered breath wave in current iteration cycle and that in the last iteration cycle is close to π, the recovered breath wave in the current iteration cycle is rotated along the time axis. The black line in Fig. 7(d) shows the rotated version. The whole breath wave recovering algorithm is shown in Algorithm 1.

**Algorithm 1**: *Breath wave recovering algorithm*

**Input**: Effective SFR Sequences, $\boldsymbol{Hs}$; Recovered breath wave in the last iteration, $BW_{Last}$.

**Output**: Recovered breath wave in the current iteration, $BW_{Curr}$.

1: normalize all effective SFR sequences to the range [-1 1];
2: $BW_{Curr} \leftarrow \boldsymbol{Hs}(1)$; /*$\boldsymbol{Hs}(i)$ denote the i-th SFR sequence*/
3: $N \leftarrow$ the amount of the SFR sequence contained in $\boldsymbol{Hs}$
4: **for** $i$ from 2 to $N$ **do**
5: **if** $\|BW_{Curr} + \boldsymbol{Hs}(i)\|_1 < \|BW_{Curr} - \boldsymbol{Hs}(i)\|_1$
6: $BW_{Curr} \leftarrow BW_{Curr} - \boldsymbol{Hs}(i)$;
7: **else**
8: $BW_{Curr} \leftarrow BW_{Curr} + \boldsymbol{Hs}(i)$;
9: **end if**
10: **end for**
11: $BW_{Curr} \leftarrow BW_{Curr}./N$;
12: **if** $\|BW_{Last} + BW_{Curr}\|_1 < \|BW_{Last} - BW_{Curr}\|_1$
13: $BW_{Curr} \leftarrow -BW_{Curr}$;
14: **end if**

The algorithm firstly normalizes effective SFR sequences (line 1). Then, it synchronizes the phase of the effective SFR sequences and synthesizes them to build breath wave (lines 2~11). We know that if two signals have the same phase, then, their superposition will strengthen, else, their superposition will weaken. Conversely, we can leverage the strength of their superposition to derive that their phases are almost the same or opposite. Based on this principle, the algorithm checks the phase of each SFR sequence and rotates the SFR sequences whose phase is almost opposite to the breath wave (the initial value of the breath wave is the first SFR sequence of effective SFR sequences (line 2)) before adding them to breath wave. (line 2~10). After that breath wave is averaged (line 11). Finally, the breath wave is rotated along the time axis if its phase is almost opposite to that of the last breath wave.

## 4 System Implementation

We implement *OmniResMonitor* on a laptop connected with an ultrasonic transceiver. The software is implemented in MATLAB. We develop a broadband multi-channel ultrasonic synchronous transceiver platform for better quality of transmitted and received signal, as shown in Fig. 8 (a). It consists of a USB sound card embedded with two broadband omnidirectional microphones (Fig.8 (b)) and a broadband speaker (Fig. 8 (c)).

The sound card uses the USB Audio Class 1.0 standard, and Fig. 8 (d) shows its key modules. The speaker is developed with an aluminum ribbon tweeter, and Fig. 8 (e) shows its key modules. Note that *OmniResMonitor* only uses a single microphone and speaker.

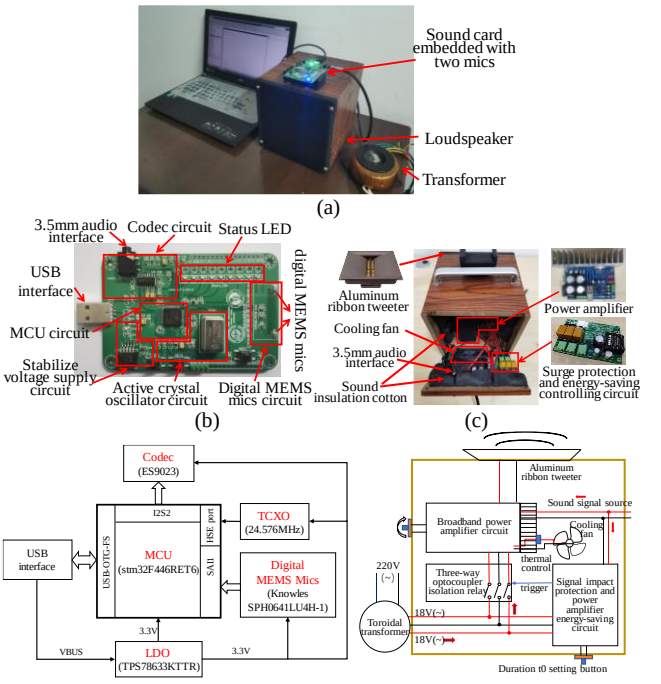


Fig. 8. Platform overview. (a) Ultrasonic transceiver platform, (b) USB sound card, (c) speaker, (d) sound card modules, (e) speaker modules.

Compared to off-the-shelf audio devices, our platform has two advantages: 1) wider frequency band and higher sampling rate. The frequency response range of our platform is 1~42kHz, while off-the-shelf audio devices have a typical band of 20Hz~22kHz. The wider available frequency band allows us to transmit and receive any types of ultrasonic signal in frequency band 20~42kHz. Our sampling rate of transmitting and receiving is able to reach 96KHz, compared to 44.1KHz or 48KHz from off-the-shelf audio devices. 2) Speaker and mic in our platform are highly synchronized because both their clocks share the same crystal oscillator. Precise clock is crucial to ensure the same sampling rate at both transmitter and receiver.

## 5 Evaluation

We now move to evaluate our system. *OmniResMonitor* runs in real time for all experiments. We compare *OmniResMonitor*'s performance with the baseline method in different scenarios, followed by evaluating its robustness by varying respiration rate, apnea, and body movement. We also conduct experiments to understand the effective sensing distance of *OmniResMonitor* under different conditions. In addition, we conduct experiments with animals (i.e., goats). Finally, we discuss the limitations of *OmniResMonitor*. The demo video of all the experiments is available at https://tinyurl.com/3mt3w7mp, https://tinyurl.com/45drar4b.

### 5.1 Experimental settings

#### 5.1.1 Key Parameters and Experimental Subjects

Transmitted signal has the following parameter settings: $f_c = 26KHz, B = 2KHz, T = 0.05s, T' = 0.1s$ (The duration of *OmniResMonitor* executing for one time is equal to $T'$).

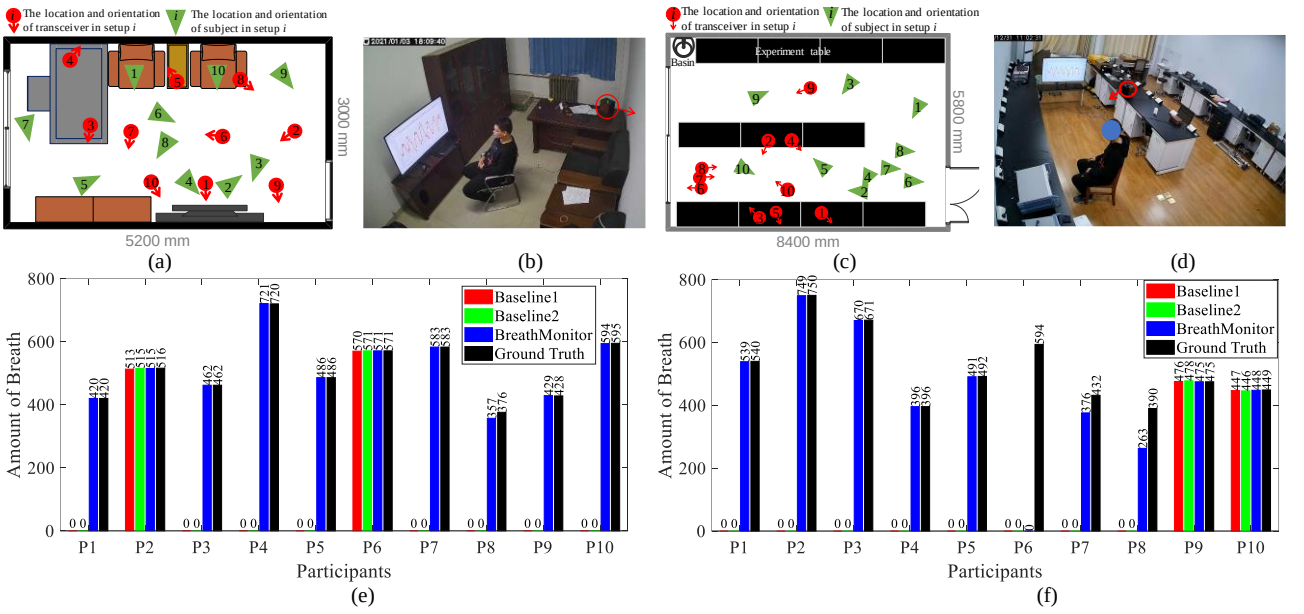


Fig. 9. Setups and results of the experiment evaluated with free location and orientation of both different subjects and transceiver in different rooms. (a) The layout of first room and the setups. Red circles linked with arrow denote the location and orientation of transceiver. Green triangles denote the location and orientation (vertex angle) of subjects (b) the photo of setup 4 in first room. (c) The layout of second room and the setups. (d) the photo of setup 4 in second room. (e) Experimental results in first room. (f) Experimental results in second room.

The sampling rate of transceiver, $f_s = 96$KHz. The power and sensitivity of the speaker are 15 watt and 94dB, respectively. The beamwidth of speaker when $f_c = 26KHz$ is $\pm 14°$. The sensitivity, signal-to-noise ratio and total harmonic distortion of the mic are -26 dBFs, 64.3 dB and 0.2%, respectively.

We recruit 20 volunteers (16 males, 4 females) aged from 21 to 27 years with a height from 1.61 to 1.81 m. We have no dress restriction, and they wear their own clothes, e.g., T-shirt, sweater, jacket and overcoat.

### 5.1.2 Baseline and Ground Truth

We compare *OmniResMonitor* with two state-of-the-art acoustic signal-based approaches [3, 45], i.e., one monitors chest movement by high resolution ranging, and the other senses the exhaled airflow by extracting the Doppler shift of the echo scattered by exhaled airflow. Both baselines require the acoustic beam to directly cover the subject's chest and the area around the subject's mouth. Additionally, the effective sensing distance of both baselines is about 1 m. They have restrictions in location and orientation for device and subject. For a fair comparison, 1) both baselines are implemented using the same devices, transmission power, and deployment scenarios; 2) we adopt the same parameter settings and configurations as specified in [3, 45].

For the ground truth, each subject is asked to wear a commercial motion sensor WitMotion WT901WIFI on the abdomen, which integrates a 3-axis acceleration sensor, a gyroscope, a 3-axis angle sensor, and a magnetometer. It accurately captures chest movement during breathing for the ground truth in each experiment.

## 5.2 System Performance Evaluation

In this section we compare our system with the two baselines in different experimental settings: 1) free location and orientation of both different subjects and transceiver in different rooms, 2) various challenging scenarios, and 3) different postures.

### 5.2.1 Free Location and Orientation of Subjects and Transceiver in Different Rooms

We first investigate the effect of different locations and orientations of subject and transceiver in two different rooms. We recruit 20 participants (16 males, 4 females). The sizes of two rooms are 5.2 m×3 m×3.5m and 8.4 m×5.8 m×3.4m, respectively. In each setup, a subject freely selects his/her location and orientation in the room. The acoustic transceiver is placed randomly, i.e., on a table, box, chair, sofa, or even on the ground. Each experiment runs for 30 minutes. This experiment is firstly conducted in the small room with 10 subjects, then we repeat it in the large room with another 10 subjects. Fig. 9(a) and Fig. 9 (c) show the room layouts, and Fig. 9 (b) and Fig. 9 (d) show the real scenarios.

Fig.9 (e) shows the experimental result in the small room. The maximum respiration monitoring error of *OmniResMonitor* is 1 breath during 30 minutes. We carefully analyze the experimental data and the recoded video and find that the error is incurred by system delay. There is an around 1s delay between actual breathing and the recovered breath wave. Two baselines work well in setups 2 and 6 shown in Fig. 9 (a), while fail in other setups. This is expected because both baselines work on directly reflected signals from the subject's chest within 1 meter, and only setups 2 and 6 meet this requirement.

Fig. 9 (f) shows the experimental result in the large room. We can see that *OmniResMonitor* achieves high accuracy in setups 1, 2, 3, 4, 5, 9, and 10, but it fails in setup 6 and does not work well in setups 7 and 8. It may be caused by the long distance between subject and transceiver. The effective sensing distance of *OmniResMonitor* for under different

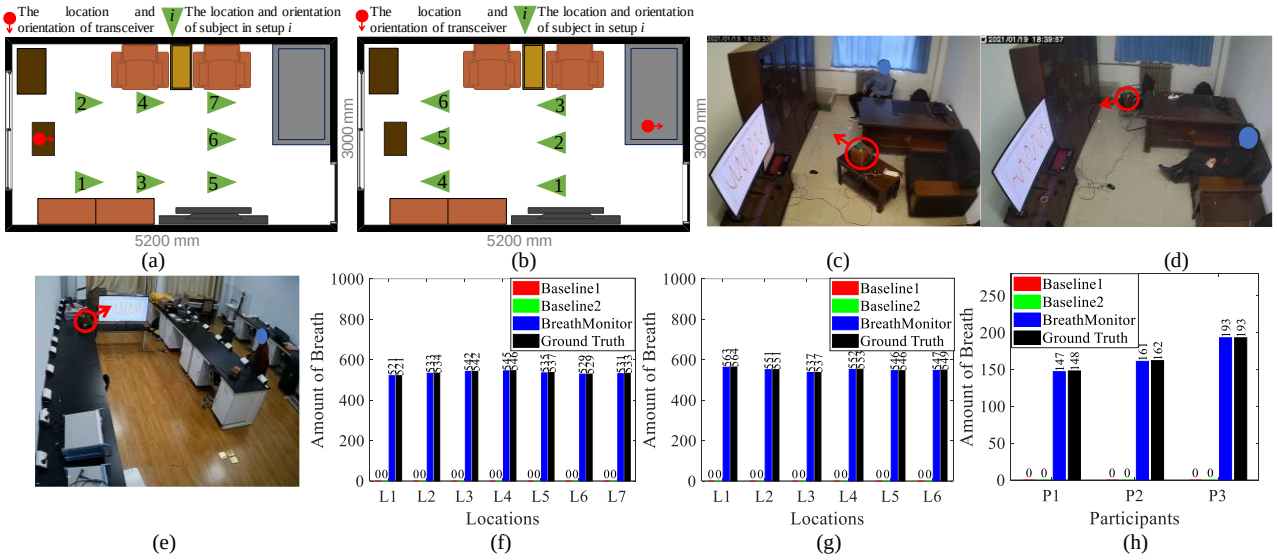


Fig. 10. Setups and results of the experiments evaluated with challenging scenarios. (a) Experimental setups of test scenario "back to face". (b) Experimental setups of test scenario "back to back". (c), (d), (e) the photos of experimental setups of test scenario that there is obstacle between subject and transceiver. (f) Experimental results of test scenario "back to face". (g) Experimental results of test scenario "back to back". (h) Experimental results of test scenario that there is obstacle between subject and transceiver.

scenarios is investigated in Sec. 5.4. As shown in Fig. 9 (c), the distance between subject and transceiver are too far (more than 6.5 m) in setups 6, 7, and 8, resulting in weak effective multipath signals. Two baselines only work well in setups 9 and 10, and fail in all other setups.

The above experiments reveal that the performance of *OmniResMonitor* is limited by the sensing range of acoustic devices. Within its effective sensing range, *OmniResMonitor* is able to achieve high accuracy without any location and orientation restriction.

### 5.2.2 Various Challenging Scenarios

In this subsection, we conduct experiments to evaluate *OmniResMonitor* in three challenging scenarios. 1) The transceiver faces toward the back of the subject at different locations – "back-to-face" scenario. 2) Transceiver and subject face opposite directions at different locations – "back-to-back" scenario. 3) There is an obstacle between subject and transceiver. The obstacle blocks the signal directly reflected from the subject's chest. As shown Fig. 10 (a), Fig. 10 (b), we evaluate *OmniResMonitor* with 7 different setups in the "back to face" scenario, 6 different setups in the "back to back" scenario. In each setup, 3 subjects are monitored for 10 minutes. Fig. 10(c), Fig. 10(d) and Fig. 10(e) show 3 different setups in the scenario that there is an obstacle between subject and transceiver. In each setup, a subject is monitored for 10 minutes.

Fig. 10(f), Fig. 10(g), and Fig. 10(h) show the experimental results in three scenarios. We observe that two baselines completely fail. It is expected since both baselines require directly reflected signals from subject's chest within 1 meter. *OmniResMonitor* achieves accurate respiration monitoring in all the scenarios with a maximum error of 2 breaths during 10 minutes.

The results indicate that abundant acoustic multipath reflection signals have been effectively exploited in *OmniResMonitor* to achieve accurate respiration monitoring in different indoor scenarios.

### 5.2.3 Different Postures

We conduct an experiment to evaluate *OmniResMonitor* when subject is lying on bed.

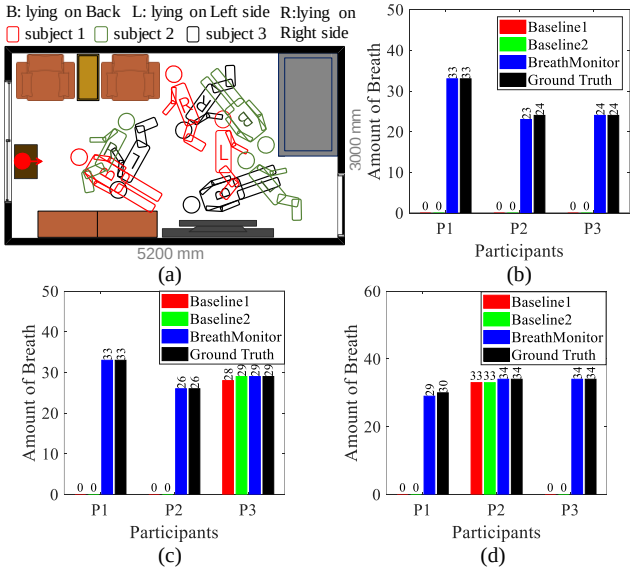


Fig. 11. Setups and results of the experiments evaluated with different sleep postures. (a) Experimental setups. (b) Experimental results when subject is lying on his/her back. (c) Experimental results when subject is lying on left. (g) Experimental results when subject is lying on right.

As shown in Fig. 11(a), a subject is asked to lie on bed with three common postures (lie on one's back, the left side and the right side). Each sleep posture is tested for 2 minutes. We repeat this experiment three times with three subjects. Fig. 11(b) shows the result when a subject is lying on his/her back. We can see that both baselines fail. Even though subject 1 is close to the device, two baselines do not

work. This is probably because the chest is almost parallel to the direction of transmitted signal propagation. The effective reflection area is small, thus the signal directly reflected from the subject's chest is very weak. In contrast, *OmniResMonitor* achieves accurate respiration monitoring for all three subjects.

Fig. 11(c) and Fig. 11(d) show the results when the subject is lying on the left and right sides, respectively. We can see that both baselines only work when subject 2 is lying on right and when subject 3 is lying on left. From Fig. 11(a), it is observed that when subject 2 is lying on right and when subject 3 is lying on left, they are close to the transceiver and their chests are completely within the coverage of the transmitted signal. *OmniResMonitor* achieves accurate respiration monitoring for all three subjects.

The experimental result indicates that *OmniResMonitor* is able to monitor breath for common sleeping postures. This is expected because it does not rely on direct reflection signals, independent to sleeping postures.

### 5.3 System Robustness Evaluation

We now conduct experiments to evaluate the robustness of the system under the conditions that are common in practice but may introduce errors in respiration monitoring.

#### 5.3.1 Impact of Respiration Rate Variation

We evaluate the respiration monitoring accuracy of *OmniResMonitor* with varying respiration rates. 5 participants are asked to change their respiration rate 5 times during 5-minute in an experiment. The lowest respiration rate of all the subjects is 9 BPM and the highest respiration rate is 29 BPM, which is outside the normal respiration rate range, i.e., 12 ~ 22 BPM.

The respiration monitoring result is shown in Fig. 12. The respiration rate variation range of each subject is represented in the rectangle above the bar. We can see that the maximum error is 3 breaths during 5 minutes.

The experimental results indicate that *OmniResMonitor* is able to accurately track both rapid and slow breathing throughout the process.

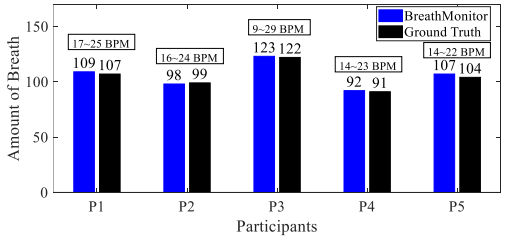


Fig. 12. Results of varying respiration rate

#### 5.3.2 Impact of Apnea

Identifying Apnea is an important objective of monitoring respiration during sleep. When Apnea happens, SFR sequence variation only comes from system internal noise, which results in very weak irregular SFR sequence variation. So, we can use the variance of the SFR sequence to identify Apnea directly. Specifically, if the variances of the first 4s subsequences (it can be adjusted according to actual need) of the selected effective SFR sequence is less than the given threshold, we can judge that Apnea happens. Note that the SFR sequence refers to the SFR sequence after detrending.

Due to the complicate ethics process with real Apnea patients in hospitals, we simulate Apnea following the clinical symptom described as "hold breath for a while" [36,43]. We recruit 5 participants to test Apnea detection performance. Each participant is asked to simulate Apnea at least 3 times during 10 minutes. There are 20 Apneas in total. The durations of simulated Apneas range from 6 to 12s. Fig. 13 shows two examples of the recovered breath wave when Apnea occurs. We can see that the recovered breath wave clearly shows Apnea. All the simulated Apneas are successfully detected.

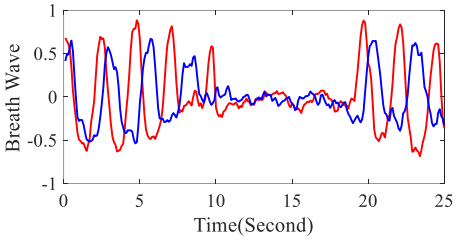


Fig. 13. Two examples when apnea happens

#### 5.3.3 Impact of Body Movement and Other Moving Objects Around

Different from Apnea, body movement or other moving objects around will generate drastic but irregular SFR sequence variation. The periodical SFR sequence variation caused by chest movement would be submerged. Under this condition, it is difficult even impossible to detect breathing. This is a common unsolved problem for all contactless respiration monitoring approaches.

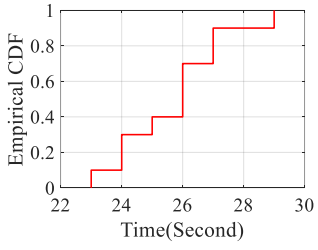


Fig. 14. CDF of the latencies from the end of the movement to the time *OmniResMonitor* resumes to monitor respiration

To reduce false alarm rate, *OmniResMonitor* is designed to suspend respiration detection once body movement is detected and recover for detecting respiration after the data generated by body movement or other moving object is flushed out from the SFR sequence buffer. We recruit 5 participants to test whether *OmniResMonitor* can actually suspend respiration monitoring when body movement occurs and resume to monitor respiration after movement stops. Specifically, during respiration monitoring, each subject is asked to change posture or stand up. In addition, another one enters the test room, then leaves the test room during respiration monitoring. Experimental results show that *OmniResMonitor* identifies all the movement and suspends respiration monitoring. Fig. 14 shows the empirical

CDF of the latencies from the end of the movement to the time *OmniResMonitor* resumes to monitor respiration automatically.

We can see that the latencies are 25 s. It is reasonable that the length of the SFR sequence buffer corresponds to about 25s. It means that the movement data will be flushed out after about 25s, the periodicity of the data will be then restored and *OmniResMonitor* automatically resumes to capture respiration. Note that even though during the latency, *OmniResMonitor* fails to capture breath, it can recover the breaths during this latency after the interfered data is flushed out from the buffer.

#### 5.3.3 Impact of Ambient Noise

Ambient noise can be received by the mic. It is necessary to test whether the ambient noise has impact on respiration detection. We test *OmniResMonitor* in several real scenarios where noise is constantly generated, i.e., 1) playing music or video in test room; 2) knocking door; 3) some one is talking loudly out the door. We recruit 4 subjects for these experiments. Experimental result show that noise has no impact on *OmniResMonitor*'s performance. The truncated SFR (refer to Sec. 3.2.2) only retains the part within the frequency band of transmitted signal, i.e., 26KHz~28KHz. In real scenarios, there is hardly any ambient noise which can reach such a high frequency band. Studies show that the highest frequency of human voice is 3KHz [40]; the highest frequency of music is 16KHz [41]; the highest frequency of the noise produced by knocking door is several hundreds Hz [42,43]. The frequencies of these ambient noise are far below 26KHz~28KHz, resulting in no effect on *OmniResMonitor*'s performance.

### 5.4 Effective Sensing Distance Estimation

To clarify the effective sensing distance of *OmniResMonitor*, we conduct an experiment to evaluate it with different setups at a distance ranging from 3 to 13m. As presented in experimental settings, the power and sensitivity of the speaker are 15 watt and 94dB, respectively. The beamwidth of speaker when $f_c = 26KHz$ is $\pm 14°$. The sensitivity, signal-to-noise ratio and total harmonic distortion of the mic are -26 dBFs, 64.3 dB and 0.2%, respectively. We test its sensing range with three setups. 1) The subject and transceiver face each other– "face to face". 2) "back to face". 3) "back to back" (please refer to section VI.B.2). For each setup, the subject is monitored for 5 minutes at each distance (from the transceiver to subject) 3, 4, …, 13m. Fig. 15 (a) shows the three setups.

Suppose the number of detected breaths is $N_{detected}$ and the number of actual breaths is $N_{actual}$, the respiration monitoring accuracy can be calculated as $R = \frac{N_{detected}}{N_{actual}}$. Fig. 15(b) shows the respiration monitoring accuracy of the above three setups. We can see that the upper bounds of effective sensing range in the three setups are 8 m, 6 m, and 5 m, respectively. Note that it does not mean that *OmniResMonitor* doesn't work beyond the distance upper bounds, but its performance may be unstable. For example, during 5 minutes tests at 10 m for the setups "face to face" and "back to face", *OmniResMonitor* can accurately monitor the subject's respiration for more than 3 minutes, while during the other 2 minutes *OmniResMonitor* fails.

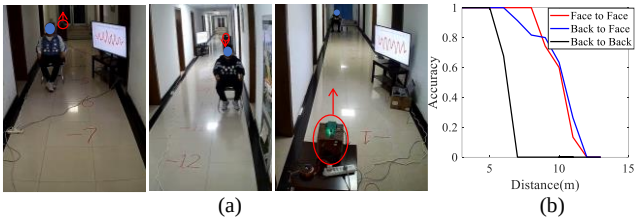


(a) (b)

Fig. 15. Effective sensing distance estimation. (a) "face to face". (b) "back to face", (c) "back to back" (d) respiration monitoring accuracy at different distances.

### 5.5 Evaluation with Animals

In this experiment, we sue this system to monitor the respiration of animals (i.e., goat) which may be useful in isolating sick goat. In our experimental setting, we have 4 goats with different ages and sizes obtained from a farming company, and a goat is free to move in the sheepfold. Since wool absorbs acoustic signals, it is challenging to monitor its respiration.

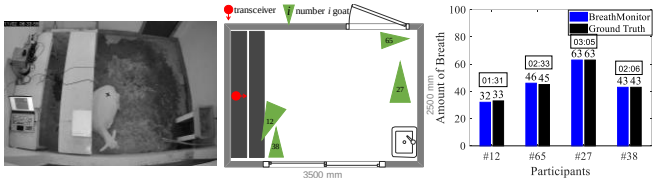


(a) (b) (c)

Fig. 16 The setups and results of the experiments evaluated with goats. (a) photo of experimental environment. (b) the location and orientation of the goats and the transceiver. (c) respiration monitoring results.

Each goat is monitored for 2 hours. During most of the time, the goats are walking around or eating. The goats are resting only for several minutes. Fig. 16 (a) shows the photo of the experimental environment. Fig. 16 (b) shows the locations and orientations when the goats are resting. The number in the triangle is the identity code of each goat sprayed on the chest. Fig. 16(c) shows the experimental results. The resting time of each goat is represented in the rectangle above the bar. We can see that, during resting, *OmniResMonitor* achieves accurate respiration monitoring for all the goats. Even though the goats no. 12 and 38 are completely blocked by the table, *OmniResMonitor* still works well.

### 5.6 Limitations

**1) Not suitable for too large rooms.** A too large room might result in weaker multipath reflection. The experiment in Section VI.B.1 reveals that *OmniResMonitor* may fail to monitor respiration due to long distance between transceiver and target, which will result in weak acoustic multipath reflection. Increasing the power of speaker or deploying multiple speakers with different orientations may be able to mitigate this problem.

**2) Single target.** The current implementation cannot be applied to monitor multiple targets. Different targets have

different respiration rates. We know that the mixture of several signals with different frequencies is aperiodic. However, *OmniResMonitor* relies on the periodicity measurement of SFR sequences. We plan to design a solution based on system impulse response (SIR) sequences in our future work. SFR integrally describes the variation of multipath reflected signals, while SIR is able to separately describe the variation of each multipath reflected signal. SIR makes it possible to identify multipath reflected signals belong to different targets according to their time delay and amplitude variation over time.

**3) Other movement events.** Other movement events will incur SFR sequences variation. In this paper, we only consider the condition that there is no other moving object in the room environment. As presented in the experiment in Section VI.C.3, *OmniResMonitor* fails when body movement and other moving events happen. To reducing false alarms, *OmniResMonitor* is designed to automatically suspend respiration detection once body movement is detected and recover respiration detecting after other movement events finish. It is worth noting that the sound interferences (such as the sound of talking, knocking on the door, playing music, etc.) will not result in SFR sequences variation. Because of the SFR truncation procedure contained in *OmniResMonitor*, only the SFR within the frequency band $[f_c, f_c + B]$ is retained, which is beyond the frequency of common sound. The movement interference is still an unsolved problem in contactless sensing which we leave for future work.

## 6 CONCLUSION

This paper presents a contactless acoustic respiration monitoring system *OmniResMonitor*, aiming to reduce the blind spot under various challenging scenarios without signal directly reflected from target's chest. Different from previous works, *OmniResMonitor* leverages abundant acoustic multipath reflection in an indoor environment to monitor a single target's respiration. Extensive experiments with both humans and animals show that *OmniResMonitor* is able to robustly monitor a single target's respiration within 5 meters in common indoor environments. Within its sensing range, *OmniResMonitor* works well under various challenging scenarios and it is indenpent to the location and orientation of target and transceiver.

## ACKNOWLEDGMENT

The authors would like to express their special appreciation to the 20 volunteers for participating in our experiments. The ethics approval has been obtained in prior to all the experiments. This work was supported in part by fellowship of China Postdoctoral Science Foundation (No. 2020M673504), Shaanxi Key Industry Innovation Chain Project(2023-ZDLNY-69), Yangling Livestock Industry Innovation Center Double-chain Fusion Project(2022GD-TSLD-46) and Australian Research Council (ARC) Discovery Project grant DP190101888.

## REFERENCES

[1] M. Mercuri et al. "2-D Localization, Angular Separation and Vital Signs Monitoring Using a SISO FMCW Radar for Smart Long-term Health Monitoring Environments," *IEEE Internet of Things Journal*. vol. 8, no. 14, pp. 11065-11077, Jul. 2021.

[2] B. Yu et al., "WiFi-Sleep: Sleep Stage Monitoring Using Commodity Wi-Fi Devices," *IEEE Internet of Things Journal*. to be published. DOI: 10.1109/JIOT.2021.3068798.

[3] T. Wang *et al.*, "Contactless Respiration Monitoring Using Ultrasound Signal with Off-the-Shelf Audio Devices," *IEEE Internet of Things Journal*, vol. 6, no. 2, pp. 2959-2973, April 2019.

[4] S. Amendola, et al., "RFID Technology for IoT-Based Personal Healthcare in Smart Spaces," *IEEE Internet of Things Journal*, vol. 1, no. 2, pp. 144-152, Apr 2014.

[5] Y. Gu *et al.*, "MoSense: An RF-Based Motion Detection System via Off-the-Shelf WiFi Devices," *IEEE Internet of Things Journal*, vol. 4, no. 6, pp. 2326-2341, Dec. 2017.

[6] https://www.who.int/news-room/q-a-detail/chronic-respiratory-diseases-asthma

[7] L. Ruvuna, and A. Sood, "Epidemiology of Chronic Obstructive Pulmonary Disease," *Clinics in Chest Medicine*, vol. 41, no. 3, pp. 315-327, Sep. 2020.

[8] J. N. Wilkinson, and V. U. Thanawala, "Thoracic impedance monitoring of respiratory rate during sedation – is it safe?" *Anaesthesia*, vol. 64, no. 4, pp. 455-456, Apr. 2010.

[9] Jaffe, and B. Michael, "Infrared Measurement of Carbon Dioxide in the Human Breath: "Breathe-Through" Devices from Tyndall to the Present Day," *Anesthesia & Analgesia*, vol. 107, no. 3, pp. 890-904, Sep. 2008.

[10] N. H. Shariati and E. Zahedi, 2005. "Comparison of selected parametric models for analysis of the photoplethysmographic signal," in *2005 1st International Conference on Computers, Communications, Signal Processing with Special Track on Biomedical Engineering*, Kuala Lumpur, Malaysia, 2005, pp. 169–172.

[11] S. Nukaya *et al.*, "Noninvasive Bed Sensing of Human Biosignals Via Piezoceramic Devices Sandwiched Between the Floor and Bed," *IEEE Sensors Journal*, vol. 12, no. 3, pp. 431-438, Sep. 2018.

[12] K. Watanabe et al. "Noninvasive measurement of heartbeat, respiration, snoring and body movements of a subject in bed via a pneumatic method," *IEEE transactions on biomedical engineering*, vol. 52, no. 12, pp. 2100-2107, Nov. 2005.

[13] M. Pastell et al., "A system for contact-free measurement of respiration rate of dairy cows," in *3rd ECPLF conference*, Skiathos, Greece, 2007, pp. 105-109.

[14] T. Kondo *et al.*, "Laser monitoring of chest wall displacement," *european respiratory journal* vol. 10, no. 8, pp. 1865-1869, Aug. 1997.

[15] P. Jakkaew and T. Onoye, "An Approach to Non-contact Monitoring of Respiratory Rate and Breathing Pattern Based on Slow Motion Images," in *2019 IEEE International Conference on Consumer Electronics - Asia (ICCE-Asia)*, Bangkok, Thailand, 2019, pp. 47-51.

[16] C. Massaroni *et al.*, "Measurement system based on RBG camera signal for contactless breathing pattern and respiratory rate monitoring," in *2018 IEEE International Symposium on Medical Measurements and Applications*, Rome, Italy, 2018, pp. 1-6.

[17] J. Penne *et al.*, "Robust real-time 3D respiratory motion detection using time-of-flight cameras," *International Journal of Computer Assisted Radiology and Surgery*, vol. 3, no. 5, pp. 427-431, Nov. 2008.

[18] D. Obeid *et al.*, "Cardiopulmonary Activity Monitoring with Contactless Microwave Sensor," in *Mediterranean Microwave Symposium*, Istanbul, Turkey, 2012, pp. 1-4.

[19] Y. Hou, Y. Wang and Y. Zheng, "TagBreathe: Monitor Breathing with Commodity RFID Systems," in *2017 IEEE 37th International Conference on Distributed Computing Systems (ICDCS)*, Atlanta, GA, USA, 2017, pp. 404-413.

[20] L. Chen *et al.*, "LungTrack: Towards Contactless and Zero Dead-Zone Respiration Monitoring with Commodity RFIDs," *Proceedings of the ACM on Interactive Mobile Wearable and Ubiquitous Technologies*, vol. 3, no. 3, pp. 1-22, Sep, 2019.

[21] Hussain *et al.*, "A cost-effective and non-invasive system for sleep and vital signs monitoring using passive RFID tags," in *MobiQuitous: Computing, Networking and Services*, New York, NY, USA, 2019, pp. 153–161.

[22] O. Kaltiokallio *et al.*, "Non-invasive respiration rate monitoring using a single COTS TX-RX pair," in *Proceedings of the 13th international symposium on Information processing in sensor networks*. Berlin, Germany, 2014, pp. 59-69.

[23] N. Patwari *et al.*, "Monitoring breathing via signal strength in wireless networks," *IEEE Transactions on Mobile Computing*, vol. 13, no. 8, pp. 1774-1786, Aug, 2014.

[24] A. D. Droitcour, O. Boric-Lubecke and G. Kovacs, "Signal-to-Noise Ratio in Doppler Radar System for Heart and Respiratory Rate Measurements," *IEEE Transactions on Microwave Theory & Techniques* vol. 57, no. 10, pp. 2498-2507, Sep 2009.

[25] R. Fletcher and H. Jing, "Low-Cost Differential Front-End for Doppler Radar Vital Sign Monitoring," In *International Microwave Symposium Digest IEEE*, Boston, MA, USA, 2009, pp. 1325-1328.
[26] Z. Yang *et al.*, "Contactless Breathing Rate Monitoring in Vehicle Using UWB Radar," in *the 7th International Workshop*, Shenzhen, China, 2018, pp. 13-18.
[27] M. Baboli *et al.*, "A new algorithm for detection of heart and respiration rate with UWB signals," in *2012 Annual International Conference of the IEEE Engineering in Medicine and Biology Society*, San Diego, CA, USA 2012, pp. 3947-3950.
[28] F. Adib *et al.*, "Smart homes that monitor breathing and heart rate," in *Proceedings of the 33rd Annual ACM Conference on Human Factors in Computing Systems*, Seoul, Republic of Korea, 2015, pp. 837–846.
[29] S. Yue *et al.*, "Extracting multi-person respiration from entangled RF signals," in *Proceedings of the ACM on Interactive, Mobile, Wearable and Ubiquitous Technologies*, vol. 2, no. 2, pp. 1-22, 2018
[30] H. Abdelnasser, K. A. Harras and M. Youssef, "UbiBreathe: A ubiqui-tous non-invasive WiFi-based breathing estimator," in *Proceedings of the 16th ACM International Symposium on Mobile Ad Hoc Networking and Computing*, Hangzhou, China, 2015, pp. 277–286.
[31] R. Ravichandran *et al.*, "WiBreathe: Estimating respiration rate using wireless signals in natural settings in the home," in *Proc. PerCom*, St. Louis, MO, USA, 2015, pp. 131–139.
[32] X. Liu *et al.*, "Wi-Sleep: Contactless sleep monitoring via WiFi signals," in *Proc. RTSS*, Rome, Italy, 2014, pp. 346–355.
[33] X. Wang, C. Yang and S. Mao, "On CSI-based vital sign monitoring using commodity WiFi," *ACM Transactions on Computing for Healthcare*, vol. 1, no. 3, pp. 1-27, May. 2020.
[34] X. Liu *et al.*, "Contactless respiration monitoring via off-the-shelf WiFi devices," *IEEE Transactions on Mobile Computing*, vol. 15, no. 10, pp. 2466-2479, Dec. 2015.
[35] J. Liu *et al.*, "Tracking vital signs during sleep leveraging off-the-shelf wifi," in *Proceedings of the 16th ACM International Symposium on Mobile Ad Hoc Networking and Computing*, Hangzhou, China, 2015, pp. 267-276).
[36] Zhang. D, Wang. H, and Wu. D, "Toward centimeter-scale human activity sensing with Wi-Fi signals," *Computer*, vol. 50, no. 1, pp. 48-57, Jan. 2017.
[37] Niu. K *et al.*, "A fresnel diffraction model based human respiration detection system using COTS Wi-Fi devices," In *Proceedings of the 2018 ACM International Joint Conference and 2018 International Symposium on Pervasive and Ubiquitous Computing and Wearable Computers* , Singapore, SG, 2018, pp.416-419.
[38] Zeng. Y *et al.*, "A full human respiration detection system using commodity Wi-Fi devices," In *Proceedings of the 2018 ACM International Joint Conference and 2018 International Symposium on Pervasive and Ubiquitous Computing and Wearable Computers* , Singapore, SG, 2018, pp.480-483.
[39] Zeng. Y *et al.*, "FullBreathe: Full human respiration detection exploiting complementarity of CSI phase and amplitude of WiFi signals,"*Proceedings of the ACM on Interactive, Mobile, Wearable and Ubiquitous Technologies*, vol. 2,no. 3, pp. 1-19, Sep. 2018.
[40] Zhang. F *et al.*, "From fresnel diffraction model to fine-grained human respiration sensing with commodity wi-fi devices,"*Proceedings of the ACM on Interactive, Mobile, Wearable and Ubiquitous Technologies*, vol. 2,no. 1, pp. 1-23, Mar. 2018.
[41] Zeng. Y *et al.*, "MultiSense: Enabling multi-person respiration sensing with commodity wifi,"*Proceedings of the ACM on Interactive, Mobile, Wearable and Ubiquitous Technologies*, vol. 4,no. 3, pp. 1-29, Sep. 2020.
[42] Liu. J *et al.*, "WiPhone: Smartphone-based Respiration Monitoring Using Ambient Reflected WiFi Signals,"*Proceedings of the ACM on Interactive, Mobile, Wearable and Ubiquitous Technologies*, vol. 5,no. 1, pp. 1-19, Mar. 2021.
[43] Nandakumar. R, Gollakota. S, and Watson N, "Contactless sleep apnea detection on smartphones," in *Proceedings of the 13th annual international conference on mobile systems, applications, and services*, Florence, Ita, 2015, pp.45-57.
[44] Min. S. D *et al.*, "Noncontact respiration rate measurement system using an ultrasonic proximity sensor," *IEEE sensors journal*, vol. 10,no. 11, pp. 1732-1739, Nov. 2010.
[45] Wang. T *et al.*, "C-FMCW based contactless respiration detection using acoustic signal," in *Proceedings of the ACM on Interactive, Mobile, Wearable and Ubiquitous Technologies*, Maui, Hawaii, USA, 2017, pp.1-20.
[46] Arlotto. P *et al.*, "An ultrasonic contactless sensor for breathing monitoring," *Sensors*, vol. 14,no. 8, pp. 15371-15386, Jun. 2014.
[47] Wang. A, Sunshine. J. E, and Gollakota. S, "Contactless infant monitoring using white noise,"in *The 25th Annual International Conference on Mobile Computing and Networking*, Los. Cabos, MX ,2019, pp.21-25.
[48] Patwari. N *et al.*, "Breathfinding: A wireless network that monitors and locates breathing in a home," *IEEE Journal of Selected Topics in Signal Processing*, vol. 8,no. 1, pp. 30-42, Nov. 2014.
[49] Wang. H *et al.*, " Human respiration detection with commodity wifi devices: do user location and body orientation matter? ," in *Proceedings of the 2016 ACM International Joint Conference on Pervasive and Ubiquitous Computing* , Heidelberg, GER, 2016, pp. 25-36.
[50] Wang. X, Yang. C, and Mao. S, "PhaseBeat: Exploiting CSI phase data for vital sign monitoring with commodity WiFi devices," in *IEEE 37th International Conference on Distributed Computing Systems (ICDCS)*, Atlanta, GA, USA, 2017, pp. 1230-1239.
[51] Wang. X, Yang. C, and Mao. S, "TensorBeat:Tensor decomposition for monitoring multiperson breathing beats with commodity WiFi,"*ACM Transactions on Intelligent Systems and Technology (TIST)*, vol. 9,no. 8, pp. 1-27, Oct. 2017.
[52] Xu, X. , J. Yu , and Y. Chen . "Leveraging Acoustic Signals for Fine-grained Breathing Monitoring in Driving Environments." *IEEE Transactions on Mobile Computing* PP.99(2020):1-1.
[53] Wan, Haoran, et al. "RespTracker: Multi-user Room-scale Respiration Tracking with Commercial Acoustic Devices." *IEEE INFOCOM 2021-IEEE Conference on Computer Communications*. IEEE, 2021.
[54] Zheng, Tianyue, et al. "More-fi: Motion-robust and fine-grained respiration monitoring via deep-learning uwb radar." *Proceedings of the 19th ACM Conference on Embedded Networked Sensor Systems*. 2021.
[55] Chen, Zhe, et al. "MoVi-Fi: motion-robust vital signs waveform recovery via deep interpreted RF sensing." *Proceedings of the 27th Annual International Conference on Mobile Computing and Networking*. 2021.

Tianben Wang received the B.S. degree in computer science from Northwest A&F University, Yangling, China, M.Sc. degree and Ph.D. degree in computer science from Northwestern Polytechnical University, Xi'an, China. He is currently an Associate Professor with the College of Mechanical and Electronic Engineering in Northwest A&F University, Yangling, China. His research interests include ubiquitous computing, contactless behavior sensing and intelligent elder assisting technology. As the leading author, he has published intensively in the top conferences/journals, including ACM UbiComp, IEEE Internet of Things Journal, IEEE TSMC-S, and ACM TIST.

Zhisheng Wang received the bachelor's degree in Mechanical Engineering from East China University of Technology, Nanchang, China, the Master degree from Northwest A&F University, Yangling, China, in 2021. He is currently pursuing the Doctor of Engineering degree in Harbin Institute of Technology, Harbin 150080, China. His research interests include embedded electronic technology and digital signal processing.

Xiantao Liu received the bachelor's degree in mechanical design manufacture and Automation from Weifang University, Weifang, China, He is currently pursuing master's degree in Mechanic Engineering in Northwest A&F University, Yangling, China. His current research interests include contactless sensing and mechanical design.


WenBo Liu received the bachelor's degree in agriculture mechanical design manufacture and Automation from Southwest University, ChongQing, China, He is currently pursuing master's degree in Mechanic Engineering in Northwest A&F University, Yangling, China. His current research interests include contactless sensing and mechanical design.

Leye Wang is an assistant professor at Key Lab of High Confidence Software Technologies and Department of Computer Science and Technology, EECS, Peking University, China. His research interests include ubiquitous computing, mobile crowdsensing, and urban computing. Wang received a Ph.D. in computer science from Pierre & Marie Curie University and Telecom SudParis, France, in 2016, and was a postdoc researcher with Hong Kong University of Science and Technology.

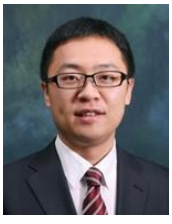

Yuanqing Zheng received the B.S. degree in Electrical Engineering and the M.E. degree in Communication and Information System from Beijing Normal University, Beijing, China, in 2007 and 2010 respectively. He received the PhD degree i n School of Computer Engineering from Nanyang Technological University in 2014. He is currently an Assistant Professor with the Department of Computing in Hong Kong Polytechnic University. His research interest includes mobile and wireless computing and RFID. He is a member of IEEE and ACM.

Jin Hu received the Ph.D degree from Northwest A & F University, Yangling, China in 2016. She is currently an Associate Professor with the Northwest A & F University, Yangling, China. Her research interest includes agricultural internet of things technology and agricultural information intelligent decision-making.

Tao Gu (Senior member, IEEE) is currently a Professor in School of Computing at Macquarie University, Australia. His research interests include Internet of Things, ubiquitous computing, mobile computing, embedded AI, wireless sensor networks, and big data analytics. He is currently serving as an Editor of IMWUT, an Associate Editor of TMC and IoT-J. Please find out more information at https://taogu.site.

Daqing Zhang (Fellow, IEEE) received the Ph.D. degree from the University of Rome "La Sapienza", Italy, in 1996. He is a Chair Professor with the Department of Computer Science and Technology, Peking University, China, and Telecom SudParis, France. His current research interests include context aware computing, urban computing, mobile computing, big data analytics, and pervasive elderly care. He has published over 280 technical papers in leading conferences and journals.

Prof. Zhang was a recipient of the Ten-Years CoMoRea Impact Paper Award at IEEE PerCom2013, the Honorable Mention Award at ACM UbiComp 2015 and 2016, the Best Paper Award at IEEE UIC 2012 and 2015. He served as the General or Program Chair for over 17international conferences, giving keynote talks at more than 20 international conferences. He is an Associate Editor for IEEE Pervasive Computing, ACM Transactions on Intelligent Systems and Technology, and Proceedings of the ACM on Interactive, Mobile, Wearable and Ubiquitous Technologies.